ELSEVIER

Nuclear Instruments and Methods in Physics Research A 455 (2000) 733–758

NUCLEAR INSTRUMENTS & METHODS IN PHYSICS RESEARCH Section A

www.elsevier.nl/locate/nima

Design considerations of a MW-scale, high-efficiency, industrial-use, ultraviolet FEL amplifier

C. Pagani[a], E.L. Saldin[b], E.A. Schneidmiller[b], M.V. Yurkov[c,*]

[a]*INFN Milano – LASA, Via Cervi, 201, 20090 Segrate MI, Italy*
[b]*Deutches Elektronen Synchrotron (DESY), 22607 Hamburg, Germany*
[c]*Joint Institute for Nuclear Research, Particle Physics Lab (LSUE) Dubna, 141980 Moscow Region, Russia*

Received 9 May 2000; accepted 18 May 2000

Abstract

Theoretical and experimental work in free electron laser (FEL) physics, and the physics of particle accelerators over the last 10 years has pointed to the possibility of the generation of MW-level optical beams with laser-like characteristics in the ultraviolet (UV) spectral range. The concept is based on generation of the radiation in the master oscillator–power FEL amplifier (MOPA) configuration. The FEL amplifier concept eliminates the need for an optical cavity. As a result, there are no thermal loading limitations to increase the average output power of this device up to the MW-level. The problem of a tunable master oscillator can be solved with available conventional quantum lasers. The use of a superconducting energy-recovery linac could produce a major, cost-effective facility with wall plug power to output optical power efficiency of about 20% that spans wavelengths from the visible to the deep ultraviolet regime. The stringent electron beam qualities required for UV FEL amplifier operation can be met with a conservative injector design (using a conventional thermionic gun and subharmonic bunchers) and the beam compression and linear acceleration technology, recently developed in connection with high-energy linear collider and X-ray FEL programs.

1. Introduction

Significant efforts of scientists and engineers working in the field of conventional quantum lasers are directed towards the construction of powerful ultraviolet (UV) lasers for industrial applications such as material processing, lithography, isotope separation, and photo-induced chemistry. Nevertheless, this problem is still unsolved: progress in this field is rather moderate and we cannot expect a significant breakthrough in the near future.

Recent investigations have shown that this problem can be solved by free electron lasers (FELs), which form a separate class of vacuum-tube devices. From this point of view it is easy to appreciate the origin of advantages of the FEL over quantum lasers. FELs predominate significantly over conventional lasers in the ability to attain a high level of average output power. In the conventional laser, the unused fraction of the pumping power (which significantly exceeds the output optical power) is dissipated in the active medium. So, the possibility of increasing the average output power is limited by

*Corresponding author. Tel: +7-096-21-62154; fax: +7-096-21-65767.

E-mail address: yurkov@sunse.jinr.ru (M.V. Yurkov).

0168-9002/00/$ - see front matter
PII: S0168-9002(00)00547-7

the heat elimination problem. By contrast, in the FEL the process of electron beam energy conversion to radiation takes place in vacuum. Utilization of the electron beam is a routine problem in the accelerator technique.

The FEL, as a device for converting net electrical power to optical power, can provide, in principle, a high efficiency close to unity. There are no physical limitations which prohibit attaining such a high efficiency and it may be achieved with appropriate development of FEL technology.

During the last decade there has been extremely rapid progress in superconducting linear accelerators, new developments in low-emittance, high-current electron injectors, and successful operation of high-precision undulators. As a result, at present there exists a technical base for the construction of powerful free electron lasers for industrial applications.

As with vacuum-tube devices, FEL devices can be divided into two classes: amplifiers and oscillators. FEL amplifiers amplify the input electromagnetic wave from the external master oscillator. The FEL oscillator can be considered as an FEL amplifier with feedback. For an FEL oscillator in the optical wavelength range the feedback is carried out by means of an optical resonator. Recently a kW-scale UV FEL oscillator project has been initiated at Jefferson Laboratory [1,2].

The main problem of constructing a high average power UV FEL oscillator is the heating effects in the cavity mirrors. Even small heat absorption can cause a change in the radius of curvature of the mirror. This leads to problems with mirror distortion, which limits the operation of a UV FEL oscillator to only the kW-level. The results of optical resonator modeling have demonstrated that the oscillator scheme for UV FEL is quite adequate for the kW demonstrator, but not scalable even to the 100 kW device [3].

If we consider the high-gain FEL amplifier, we find that there are no thermal loading limitations to increasing the average output power of this device up to the megawatt level. Since the amplification process develops in vacuum during one pass of the electron beam through the undulator, the problem of absorption of radiation in the cavity mirrors does not exist at all.

In this paper we perform design consideration of a MW-scale UV FEL amplifier. The technical approach adopted in this design makes use of a superconducting RF linear accelerator (SRF accelerator). The primary motivation for adopting this approach was to meet simultaneously the requirements for high average power and high net efficiency. Typically only about a few per cent of the electron energy is converted to light. With a SRF linac, an FEL amplifier would acquire high average power, owing to the input beam's continuous-wave (CW) nature. The energy recovery of most of the driver electron beam's energy would further increase the power efficiency.

The FEL amplifier is driven by a 1 GeV electron beam, prepared with phase-space properties to allow high-gain amplification in the undulator, an injector, an SRF electron linac, and a carefully designed bunch compressing system. At this relatively high energy of the driving electron beam, two beam parameters are essential to reach high gain within a not too long undulator: a small transverse beam emittance to provide both small beam transverse size and small angle divergence in the undulator, and small longitudinal emittance to achieve high instantaneous beam current at small energy spread. During the last decade there has been extremely rapid progress in the development of injection systems for linear accelerators, in particular in the high-energy bunch compression system, because it is an essential component of future Linear Colliders and X-ray FELs [4,5]. As a result, it became possible to produce electron beams which can be used as driving beams for high-power UV FEL amplifiers.

A lower electron energy, say about 100–150 MeV, seems to be more natural for the generation of the UV radiation. However, during the optimization of the MW-scale FEL we have chosen the electron energy be around 1 GeV. Such a choice allows us to solve simultaneously several complicated technical problems. First, we can decrease the average current of the driving electron accelerator down to the value around 10 mA, while keeping the average power of the radiation in the MW range. The value of 10 mA is quite tolerable for modern SRF linacs. The requirements for the parameters of the injector also become moderate. As a result, we

can use the injector, consisting of a conventional thermionic gun, subharmonic prebunchers and preacceleration SRF cavity, which is practically identical to that designed at LBL for the CW-mode operation infrared FEL oscillator [6].

The FEL amplifier described in this paper provides, in range 260–500 nm, a continuous train of 1 ps micropulses, with 80 mJ of optical energy per micropulse at a repetition rate of 6.1 MHz. The average optical output power can exceed 500 kW. In this conceptual design we assume the use of a conventional quantum generator as a master laser, which provides a continuous train of 10 ps micropulses, with 100 nJ of optical energy per micropulse. The average output power of the master laser is about 1 W. A dye laser system pumped by the second harmonic of a Nd glass laser can be used for this purpose.

The industrial surface processing is one of the most promising fields for application of high-power UV FEL. A MW-scale coherent light source with variable wavelength could tailor the surface characteristics of polymers, composites, ceramics, and metals for use in manufactured products. In the deep UV range (below 300 nm), application to photo-induced chemistry, microlithography, and other semiconductor manufacturing also has high potential [7].

The attractive features of UV FEL amplifier are the ultrashort pulse, high peak power and high repetition rate. Recently a highly efficient isotope enrichment process was observed directly in laser-ablation plumes generated from ultrafast laser pulses focused on the solid surface [8]. Ablation is initiated by a Ti : sapphire chirped-pulse laser amplifier. It is worth to mention that the parameters of the optical pulses, relevant for this application (i.e. duration and peak power), are similar to the table-top TW-scale laser and to the FEL discussed here. On the other hand, the repetition rate of the free electron laser is by many orders of magnitude higher. So, application of a MW-scale FEL could provide a novel and cheap tool for industrial-scale isotope separation. For instance, it is possible to use this technique to make isotopically pure thin films of semiconductors, which are known to have an improved ability to conduct heat, a key requirement for today's densely packed computer chips [9]. Thus, we can expect that the commercial potential of a powerful UV FEL amplifier would also include isotope separation.

The wall plug power to output optical power efficiency of a FEL for industrial applications is an important criterion. For the present design we fixed on a rather conservative value of the FEL amplifier efficiency (i.e. the ratio of the energy in the radiation pulse to the energy in the electron pulse) of about 4%. Energy recovery of most of the driver electron beam energy would increase the power efficiency. However, one should take into account an important problem of the induced energy spread in the electron beam at the exit of an FEL amplifier which can significantly limit the possibilities of energy recovery. In the present design this problem is solved in the following way. The initial energy of the electron beam is about 1 GeV. The energy spread of the electron beam after leaving the undulator is pretty large, about $\pm$ 50 MeV. An important feature of our design is that a very short electron bunch (of about 0.15 mm rms) is used for the generation of the radiation. When the electron bunch leaves the undulator, we apply a transformation of the particle distribution in the longitudinal phase space resulting in increased bunch length and decreased energy spread (this technique is similar to that used for bunch compression [10]). The scheme is realized as follows. After leaving the undulator the electron beam passes a special dispersion section. The length of the bunch is increased by a factor of about 30, and the uncorrelated energy spread is transformed to one correlated with the position of the particles in the bunch. The resulting electron bunch length is still tolerable for use in the energy recovery scheme. Subsequently, the electron bunch passes a special accelerating structure with off-crest phase (RF lens), and the energy spread of the electron beam is reduced to about 2 MeV. The electron bunch with such energy spread can be decelerated safely down to the energy of about 10 MeV, which is much less than the initial energy spread. As a result, the efficiency of the energy recovery system is increased significantly, and we can reach the RF power to output optical power efficiency of about 80%. The efficiency of the conversion of AC power into RF power is given by $\eta(\mathrm{AC} \rightarrow \mathrm{RF}) = \eta(\mathrm{klystron})\eta(\mathrm{modulator})$, where $\eta(\mathrm{klystron})$ is the

electronic efficiency of the klystron and η(modulator) is the efficiency of the klystron modulator. Assuming the efficiency of the modulator be η(modulator) = 80%, and the electronic efficiency of the high-power CW klystron η(klystron) = 60%, we obtain that the AC wall plug power to output optical power efficiency is about 40% (not taking into account cryogenic losses). In our conceptual design, energy recovery reduces the required linac RF driver power by a factor of 20, and the dissipated power in the beam dump by a factor of 95. Another source of the energy consumption is cryogenic system of the SRF accelerator. The present design requires cooling of about 30 cryomodules. To do this, we need a He refrigerator with net power consumption less than 1 MW. As a result, we obtain a total efficiency of the proposed UV FEL amplifier equal to 20%. It is also relevant to keep in mind the problem of radio-nuclide production in the dump. In the present design the beam dump energy is below the photon–neutron production threshold, so this problem does not exist.

The paper proceeds as follows. In Section 2 we describe the basic ideas of the proposal, in particular the bunch compression scheme for the FEL amplifier and the energy bunching for the energy recovery system. Section 3 is devoted to the description of the accelerator and the transport optics necessary to produce an electron beam suitable for an industrial-use UV FEL.

The conceptual design of the high-gain UV FEL amplifier with a tapered undulator is described in Section 4. Optimization of the parameters of the FEL amplifier has been performed with the nonlinear three-dimensional time-dependent simulation code FAST [11]. This code, as well as other codes, such as GINGER [12] and GENESIS [13], has been developed in the framework of the investigations on X-ray free electron lasers [14,4,5]. Recently the reliability of the code FAST has been demonstrated by means of the numerical simulation of the high-gain FEL amplifier starting from the shot noise [15,16].

The energy-recovery system is of critical importance to the overall performance of the FEL amplifier. The electron beam stability requirements at the undulator entrance, based on the overall energy-recovery system requirements, are summarized in Section 5.

Section 6 deals with a design strategy for the UV FEL undulator. The tapered undulator for an industrial-use UV FEL amplifier needs to be rather long in order to provide the required power of the output radiation. The maximum length in our case is 60 m. Thus, strong focusing elements are needed for the electron beam transpor system. A combined function undulator (CFU) approach, to implement strong focusing in a long undulator, is discussed. In this section tolerances for field errors and alignment are estimated on the basis of work done for the 30 m long CFU undulator for the VUV FEL at the TESLA Test Facility [17].

Section 7 discusses the output optical system for the high average power amplifier. An important problem is that of extracting the powerful laser beam into the atmosphere. To solve this problem, we propose to use a long extractor with differential evacuation from the operating vacuum of the accelerator to atmospheric pressure. Helpful factors for application of this technique are small transverse size, about 1 mm, and small angle divergence, about 10 microradians of the output radiation. Expanding the laser beam after extracting into the atmosphere is a routine problem. Grazing incident mirror optics can be used for this purpose. Thus, the problem of output window damage does not exist.

Section 8 is devoted to a possible scenario for the power upgrade. The average output optical power of the UV FEL amplifier is clearly limited by the average current achievable with the injector and superconducting cavities. In order to go to power beyond $P_{\mathrm{av}} \simeq 0.5$ MW, the repetition rate of the injector would therefore have to be increased. The upgrade would provide a maximum average power of $P_{\mathrm{av}} \simeq 2$ MW. The injector and driver accelerator are designed such that the power upgrade can be accommodated without further significant hardware modification. Finally, this section also describes the basic ideas of the photon energy upgrade. One big attraction of the FEL amplifier scheme is the absence of apparent limitations which would prevent operation at even the VUV wavelength range. It is demonstrated that the FEL amplifier has the capability of maintaining

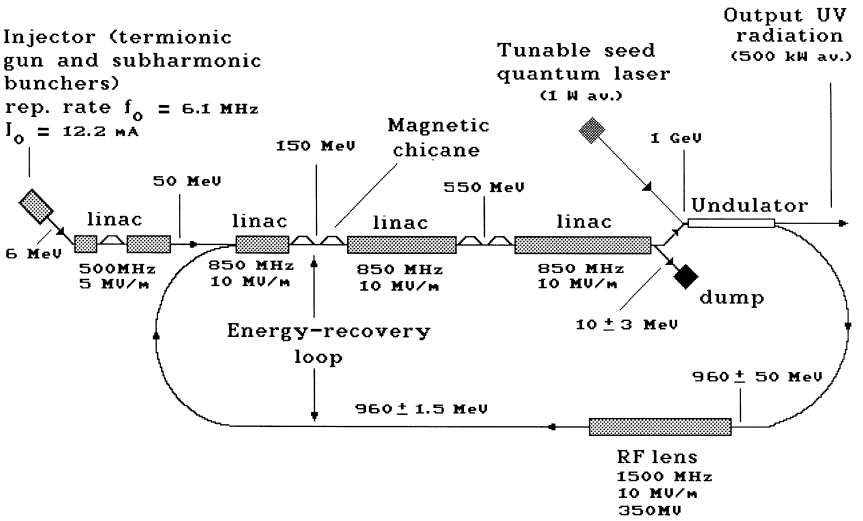

Fig. 1. Schematic illustration of design configuration for the UV FEL amplifier.

MW-scale output optical power at a wavelength well below 200 nm. A new injector system and master laser oscillator would have to be constructed.

When considering a possible technical realization of the injector, driver accelerator structure, and energy recovery system, we have used only those technical solutions which have been used (or are planned to be used) elsewhere. Many components of the proposed equipment have been demonstrated in practice. However, till now there is no operating FEL amplifier with the parameters close to those required. So, the basic idea of the proposal, namely a possibility to construct a high-gain UV FEL amplifier with a tapered undulator at the energy of the driving electron beam of about 1 GeV, requires experimental verification. To perform such a verification, there is no need to build a full-scale facility. It should be noted that an FEL amplifier is a single bunch scheme. As a result, it is possible to use an accelerator with any electron beam pulse format. One only needs the electron bunch to have parameters similar to those for designed UV FEL amplifier. An accelerator facility with electron bunch parameters practically identical to those required is being developed, for instance, in the framework of the superconducting linear collider project TESLA [4]. A 1 GeV SRF linear accelerator, under construction at the Tesla Test Facility (TTF) at DESY, will produce an electron beam with high peak current (2.5 kA), low emittance ($\varepsilon_n \simeq 2\pi$ mm mrad.), and energy spread ($\sigma_E \simeq 0.1\%$). The main practical application of this accelerator is to use it for driving the soft X-ray SASE FEL. In principle, it would be possible to install an additional FEL beamline in the same tunnel in parallel with the soft X-ray FEL. The UV FEL would use the same electron beam as the X-ray FEL, thus providing minimal interference between these two options [18]. UV FEL at TTF will provide peak and average output power up to 200 GW and 7 kW, respectively. A 10 kW-scale UV FEL amplifier would demonstrate the technology, and an array of user laboratories would allow development of the prospective industrial applications.

2. Facility description

Fig. 1 shows the general scheme of the MW-scale FEL amplifier driven by a 850 MHz SRF linear accelerator. In the acceleration sections, the superconducting cavities are designed to operate with nominal accelerating gradients of 10 MV/m.[1] The

[1] The accelerating gradient defines only the length and cost of the accelerator, but not the characteristics of electron beam.

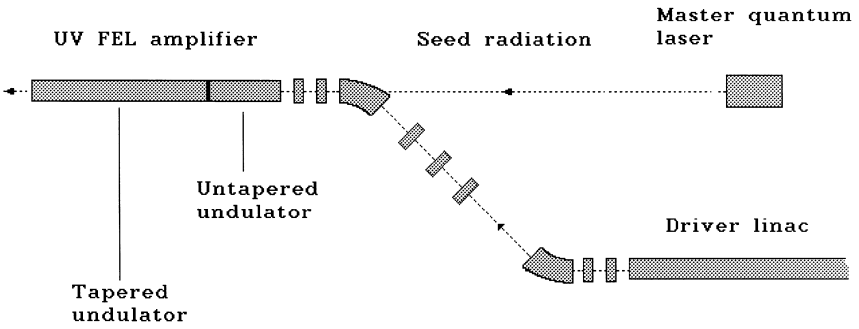

Fig. 2. Basic scheme of the MOPA laser system.

electron beam originates in a high-voltage DC gun with gridded thermionic cathode. The injector includes two subharmonic, room-temperature buncher cavities and a 500 MHz accelerating module. The injector produces 6.5 MeV electron pulses with a duration of 33 ps (FWHM), at average current 12.2 mA (2 nC of charge, 6.1 MHz repetition rate). The bunched low-energy electron beam then enters the SRF linac for further acceleration up to energy of 1 GeV. The accelerated beam enters the undulator, yields light, and finally decelerates through an energy recovery pass in the SRF linac before its remaining energy is absorbed in the beam dump at the final energy of about 10 MeV.

The FEL provides a continuous train of 1 ps micropulses, with 80 mJ of optical energy per micropulse at a repetition rate of 6.1 MHz. The average optical output power can exceed 500 kW. The FEL is based on the principle of a master oscillator–power amplifier (MOPA) scheme (see Fig. 2). The key advantage of the MOPA scheme compared to the FEL oscillator scheme is that neither mirrors nor dispersion elements forming an optical cavity are required. Thus, no known technical limitation would prevent operation even up to the megawatt average output power level. In this conceptual design we assume the use of a conventional quantum generator as master laser (wavelength range 260–500 nm, pulse duration 10 ps, energy per pulse 100 nJ, repetition rate 6.1 MHz). A dye laser system pumped by the second harmonic of a Nd glass laser can be used for this purpose (see Fig. 3). Radiation from the master laser will be amplified in the FEL amplifier with a tapered undulator providing an extraction efficiency (ratio of the energy in the output radiation pulse to the energy in the electron pulse) of about 4%. The basic parameters of the UV FEL amplifier are given in Table 1.

A driver linac design with energy recovery requires considerable manipulation of the longitudinal and transverse beam dynamics in order, on the one side, to provide the bunch parameters for effective generation of the radiation, and on the other side, to make effective energy recovery feasible. A relatively high value of peak beam current is needed in the undulator to reach high-gain amplification within a reasonable undulator length. In our design this value is about 1.5 kA, corresponding to 0.15 mm rms bunch length for a 2 nC bunch charge. This value is not attainable directly in the injector, because space-charge forces would blow up both the transverse beam size and the energy spread. Thus, the use of magnetic bunch compression at higher energy is foreseen in order to reduce the bunch length.

In an ideal bunch compressor, a linear correlation between energy and longitudinal position is induced in the bunch, by passing a RF accelerator structure with off-crest phase. Then there follows a sequence of bending magnets where particles with different energies have different path lengths. As a result the bunch tail has a shorter path and can catch up with the head, effectively compressing the bunch. Compressing the bunch in the acceleration system will be done in stages to avoid two effects limiting the bunch length achievable. On the one hand, compressing the bunch late in the linac

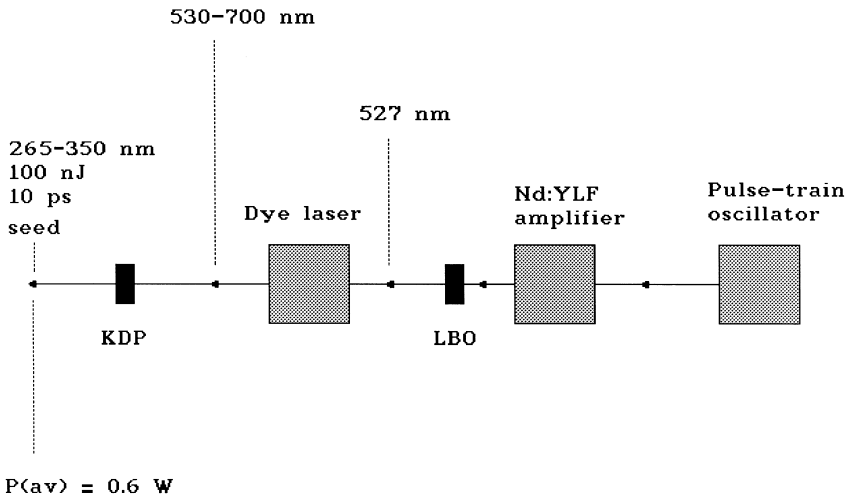

Fig. 3. Scheme of the master laser providing permanent tuning in the wavelength range 265–350 nm.

Table 1
Performance characteristics of the UV FEL amplifier

Electron beam	
Energy (MeV)	1000
rms energy spread (%)	0.2
Bunch charge (nC)	2
rms pulse duration (ps)	0.5
Micropulse repetition rate (MHz)	6.1
normalized emittance (π mm mrad)	8
Undulator	
Type	Planar, Sm-Co/steel
Period (cm)	7.0
Gap (mm)	12
Maximum peak field (entr./exit) (T)	1.15 / 1.05
No. of undulator periods	850
External beta-function (m)	3.0
Radiation	
Wavelength (μm)	260–500
Spectrum width	Transform-limited
Peak power (GW)	110
Average power (MW)	0.5
Micropulse duration (ps) (FWHM)	0.7
Micropulse energy (mJ)	83
Repetition rate (MHz)	6.1

accumulates too much non-linear (although correlated) energy spread from the cosine-like accelerating field. On the other hand, compressing early at relatively low energies would induce too much non-linear correlated energy spread due to space-charge effects.

In the present design uncorrelated energy spread of the beam leaving the injector is around 75 keV rms, the length is 4.2 mm rms. The FEL amplification process requires less than 3 MeV rms energy spread at the undulator entrance. The initial longitudinal emittance of about 0.3 MeV mm is already close to the finally tolerable emittance, so emittance blow up during compression has to be kept small.

In principle, one could consider performing the bunch compression in one step at an energy level, where space charge is not critical anymore. However, even at comparatively low RF frequency (850 MHz), the curvature of the accelerating field would then impose an intolerable non-linear correlated energy distribution along the bunch. The proposed solution is to perform compression in three steps: at 30 MeV (from 4.2 to 1.6 mm rms), 150 MeV (from 1.6 to 0.45 mm rms) and 550 MeV (from 0.45 to 0.15 mm rms). All bunch compressors are simple chicanes formed of four rectangular dipole magnets with matching quadrupoles only before and after the bending magnets. The last part of the linac accelerates the bunch with an on-crest phase up to one GeV.

In our conceptual design we assume the use of an energy-recovery system. Only about 4% of the electron's energy is converted to light. The remainder undergoes energy recovery, being returned to the SRF cavities, where most of it is converted back to

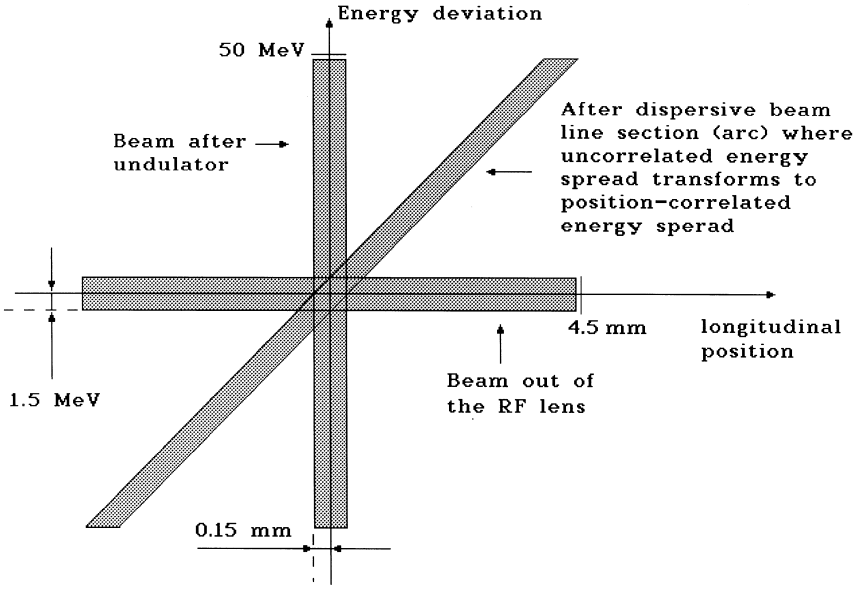

Fig. 4. Principle scheme of required energy compression (linear approximation).

RF power at the cavities' resonant frequency. The decelerated beam is then dumped. The SRF linac must decelerate the bunches from an energy of about 960 MeV to about 10 MeV in the beam dump. For such deceleration, the energy spread of the electrons in the SRF linac cannot be larger than $\Delta E_f \simeq \pm 3$ MeV. This value is not attainable directly from the FEL amplifier, because at the exit of the undulator, the electron beam has a large induced energy spread of about $\Delta E_i \simeq \pm 50$ MeV which is comparable to the average energy losses. Thus, the use of energy bunching is foreseen in order to reduce the energy spread from 50 down to 3 MeV.

Fig. 4 shows the principle of energy compression in longitudinal phase space. Energy bunching is appropriate for the situation in which particles are bunched tightly in phase, but have a large energy spread [10]. A similar situation occurs at the undulator exit. The transformations are in the reverse order from those used for phase bunching. A relation is first established between phase and energy, creating a skew "ellipse" in phase space. This is followed by a RF lens that reduces the energy spread by applying a reverse voltage that returns the "ellipse" to axis. Phase separation (i.e. linear correlation between energy and longitudinal position) can be obtained in our case by the first, 180° bend of the recovery loop. Passing this bend, particles with different energies have different path length; mostly because they travel on orbits with different radii through the bending magnets with dispersion. The dependence between path length and particle energy is therefore, to a very good approximation, linear. A correlated energy spread in the bunch is cancelled by passing a RF structure at 90° crossing phase (0° corresponding to running on-crest). The linear portion of a cosinusoidal voltage can approximate the linear lens quite closly. If we expand the RF cavities voltage about a phase $\Delta\phi = (\phi - 90°)$, we obtain

$$V = V_0\Delta\phi - V_0(\Delta\phi)^3/(3!)$$

where the linear portion $V_0\Delta\phi$ is the voltage necessary to return the skew "ellipse" to the axis. From consideration of phase space we obtain

$$\Delta E_f = \Delta E_i \Delta\phi_i/\Delta\phi_f$$

where $(\Delta E_i, \Delta\phi_i)$ and $(\Delta E_f, \Delta\phi_f)$ are the initial and transformed energy and phase spreads. In our case $\Delta E_f \ll \Delta E_i$ and we can use the approximation that the linear portion of the reverse voltage is just

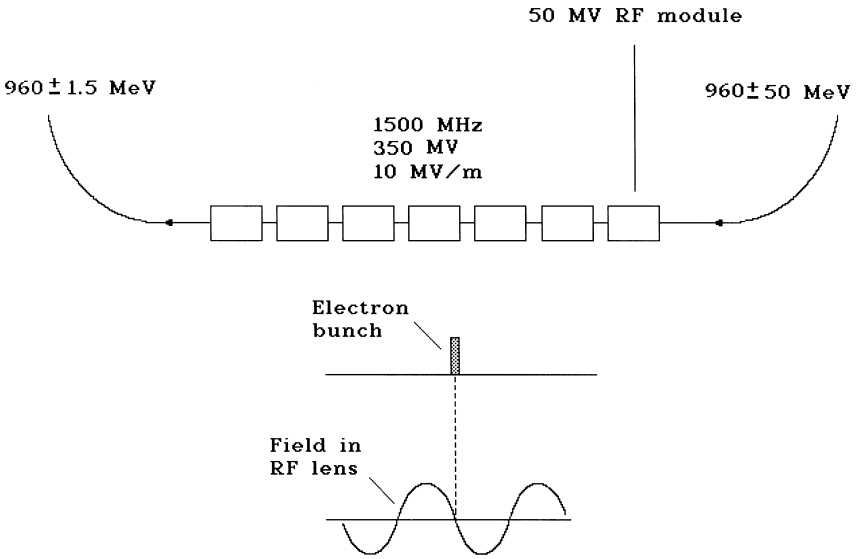

Fig. 5. The scheme of operation of the RF lens.

sufficient to cancel the mean value of the initial energy spread ΔE_i, that is

$$eV_0\Delta\phi_f = \Delta E_i.$$

The effect of the first non-linear term is to distort the phase distribution which results in "effective" energy spread

$$(\Delta E_f)_{eff} \simeq \Delta E_i \Delta\phi_i/\Delta\phi_f + \Delta E_i(\Delta\phi_f)^2/(3!).$$

The proposed energy bunching system is sketched in Fig. 5. After leaving the undulator the beam enters the phase debuncher. This debuncher is basically part of the 180° bend of the energy recovery loop. It is relevant to comment on the definitions of the energy spread at the undulator exit and the bunch length after the debuncher. It is shown in Section 4 (see Fig. 14) that the energy distribution of the electron beam at the exit of the undulator is a complicated one consisting of two maxima. However, the peculiarity of this distribution is that it falls sharply to zero at the edges. It is natural to describe such a distribution not by the rms value, but the total width. In the following we use the total width of this distribution, ΔE_{tot}, which contains almost all particles. The center-of-mass of the distribution is only slightly shifted from the mean value, so we will assume for the further estimations that the particles are distributed in the interval $\Delta E_i = \pm \Delta E_{tot}/2$. After leaving the debuncher the bunch length is increased by a factor of few tens, and uncorrelated energy spread transforms to one correlated with the longitudinal position of the particles in the bunch. The shape of the longitudinal density distribution of the bunch is similar to that of the initial energy distribution. Due to this reason it is also convenient to describe the bunch length not by the rms value, but by the total bunch length, Δz_b. In our design of the debuncher specified output bunch length is about $\Delta z_b \simeq 9$ mm.

The design of a RF structure for RF lens is based on the need to minimize voltage V_0 and nonlinearity of the RF length. On the other hand, there exist problems of maximizing the stability of the energy bunching system operation and minimizing of the cost. As a result, we select 1500 MHz structure, based on standing-wave superconducting cavities operating at the gradient of 10 MV/m. The transformed phase spread corresponding to this RF frequency is about $\Delta\phi_f = \pi\Delta z_b/\lambda_{rf} \simeq 0.14$, and ratio $\Delta\phi_f/\Delta\phi_i$ is about 30. For chosen parameters of the FEL amplifier we get induced energy spread $\Delta E_i \simeq \pm 50$ MeV. Voltage V_0 which is sufficient to

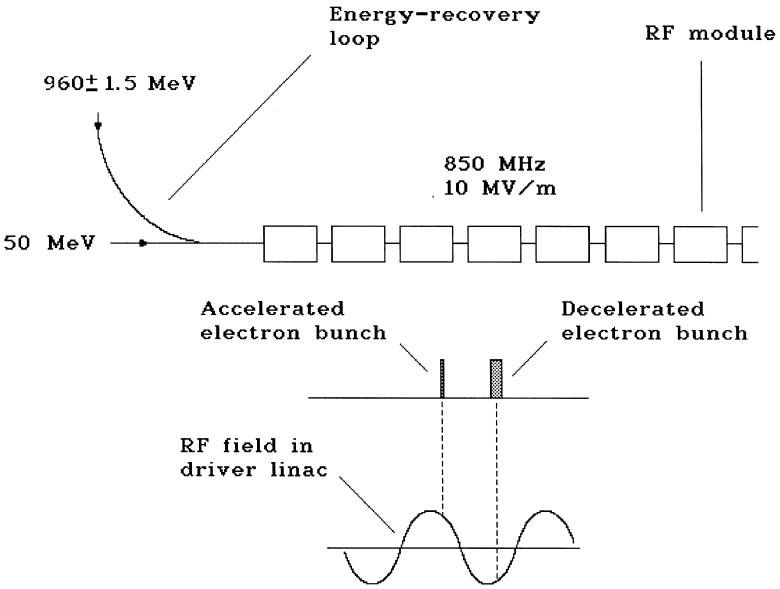

Fig. 6. The scheme of operation of driver linac.

cancel the mean value ΔE_i is equal to $V_0 \simeq 350$ MV. The transformed energy spread and its distortion are about $\Delta E_f \simeq \Delta E_i \Delta\phi_i/\Delta\phi_f \simeq \pm 1.5$ MeV and $\Delta E_d \simeq \Delta E_i(\Delta\phi_f)^2/(3!) \simeq \pm 0.2$ MeV, respectively.

It should be noted that energy bunching, in our case, can be treated by single-particle dynamic theory. This situation is in marked contrast to phase bunching, in which the space charge and wake field effects determine the effective phase-space area occupied by the particles.

The second arc transport from the undulator to the driver linac is isochronous. After passing this arc the beam is decelerated in the first part of the driver linac at an off-crest phase from the energy roughly 960–550 MeV. Finally, it enters the last part of the linac which decelerates the bunch with an on-crest phase down to energy of 10 MeV. An off-crest deceleration phase should be tuned in order to minimize the RF power consumption by the accelerator (see Fig. 6). Since the length of the decelerated bunch is relatively large, one should avoid induced correlated energy spread. Linear fraction of this energy spread can be cancelled by means of changing the off-crest phase at different stages of deceleration. The driving electron beam is accelerated with the off-crest phase ϕ_0 in the first part of the linac ($\phi_0 = 0^\circ$ corresponds to running on the crest), then if we take the phase of the decelerating electron beam $\phi_d = (180^\circ - \phi_0)$, the bunch head is at lower energy than bunch tail. At some point of accelerator (between the second and the third bunch compressor) we change the phase of decelerating beam by $\phi_d = (180^\circ + \phi_0)$ with the bunch head at higher energy than the bunch tail. Such a phase shift can be done in the isochronous bypass providing lengthening of the path of the decelerated bunch (path difference is of about 3 cm at $\phi_0 \simeq 20^\circ$). So, the linear fraction of the correlated energy spread is cancelled. However, quadratic non-linearity of the RF field cannot be cancelled and leads to the additional increase of the energy spread by the value of $\Delta E_d \simeq \pm 1.5$ MeV. As a result, at the dump energy of $E_{dump} \simeq 10$ MeV effective energy spread is about $\Delta E_f \simeq \pm 3$ MeV.

3. Accelerator systems

3.1. Injector system

The arrangement of injector is shown schematically in Fig. 7. The injector starts with a 300 kV

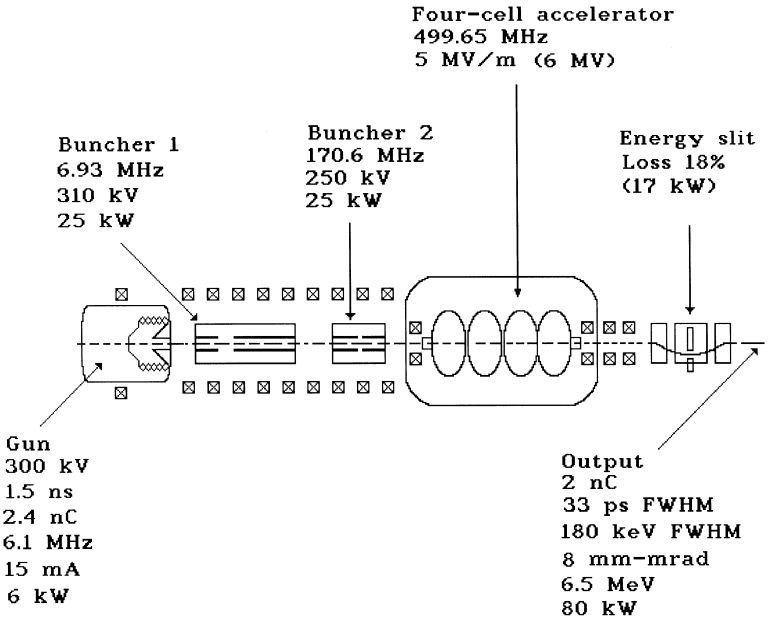

Fig. 7. Schematic of the UV FEL amplifier injector.

grid-controlled thermionic gun as a source. The gun produces 2.5 nC pulses with a duration of 1.5 ns. A 2 cm^2 thermionic cathode provides the needed current. The bunch compression is performed by means of a sequence of three bunchers operating at fundamental frequencies of 61, 171 and 500 MHz. The 500 MHz buncher is a superconducting structure and the other two operate at a room temperature.

Both subharmonic bunching cavities use quarter-wavelength coaxial cavities operating at the fundamental TEM mode. A chicane with a high-power energy slit capable of a scraping up to 25% of the beam is needed between the injector and accelerator. The slit removes electrons in the tail of the spectrum more than 180 keV (FWHM) below the mean of the energy distribution. Details regarding bunchers design and their operating parameters can be found in Ref. [6].

The injector is followed by a 500 MHz SRF booster cavity which increases the beam energy to 30 MeV. Downstream of this cavity a magnetic chicane bunch compressor decreases the bunch length by about a factor of three to $\sigma_z \simeq 1.6$ mm. The first magnetic bunch compressor might be considered as a part of the electron injector, since it is located directly after the booster cavity (see Fig. 8). The bunch is compressed by accelerating in booster cavity with an off-crest RF phase, thereby introducing a correlated energy spread along the bunch. This is followed by a bending section (chicane) with linear path length dependence on particle energy.

3.2. Driver linac system

The superconducting linear accelerator is an ideal accelerator to drive a high average power FEL amplifier. There are two main reasons. First, a superconducting accelerator provides a high-energy efficiency. Second, the stability requirements of the high average power electron beam dictate the use of low-frequency superconducting RF structures and CW operation. CW operation of SRF cavities allows more time for feedback control.

The field of superconducting RF linac design is developed rapidly, and gradient of 10 MV/m is now considered as a routine one. Selected parameters for operating superconducting accelerators are

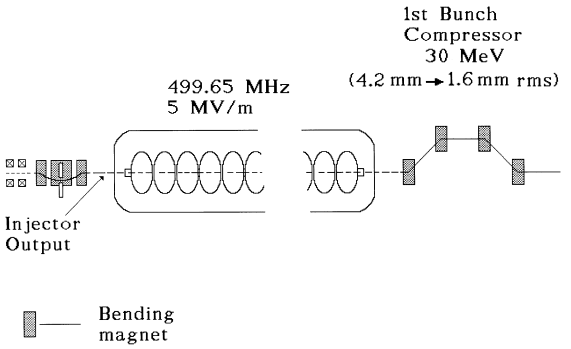

Fig. 8. Layout of the bunch compressor at stage 1.

Table 2
Selected parameters for operating superconducting linear accelerators

	Frequency (MHz)	Gradient (MV/m)	Current (mA)	Q_0
Cornell (CESR)	1500	8	20	5×10^9
DESY (HERA)	500	5	40	10^9
CEBAF (DEMO)	1500	10	10	6×10^9
DESY (TESLA)	1300	25	8	5×10^9

presented in Table 2. Niobium cavities are installed in the electron–positron storage rings LEP (CERN), CESR (Cornell), TRISTAN (KEK) and HERA (DESY), and successfully used with operating gradient 3.5–4.5 MV/m. The largest SRF system is assembled in the Jefferson Laboratory (CEBAF linac) which operates with the gradient of about 8 MV/m. The cavities for these machines have been produced by industry.

DESY is now developing the superconducting RF technology which will provide the basis for the construction of the large electron–positron collider with integrated X-ray laser sources. These activities are carried out within the framework of the large international TESLA collaboration. The challenge of the project is in pushing the superconducting linac technology to a high accelerating gradient and at the same time reducting the cost per unit length. TESLA uses niobium cavities cooled by superfluid Helium to $T = 2$ K and operating at L-band frequency (1.3 GHz). The design gradient for linear collider is 25 MV/m with an unloaded quality factor of $Q = 5\times10^9$. In order to demonstrate the feasibility of the SRF cavity technology, the TESLA collaboration started an R&D program of constructing the TESLA Test Facility [19]. At this time TTF cavities had reached average gradient of 20 MV/m. A test linac is under construction in order to demonstrate the beam acceleration up to 1.2 GeV [4].

The frequency choice for the driver accelerator was based predominantly on stability consideration: low frequency implies large transverse dimensions and larger cavity volume. Thus, the cavity stores more energy, relative to the beam, and wake-field effects are minimized – both of which improve stability. Cavities in the 350–500 MHz regime are in use in the electron–positron storage rings. However, for one GeV industrial-use linac the niobium and cryostat costs for these cavities are prohibitive. In addition, at a higher-frequency cryogenic losses are lower. Hence, a higher frequency has been chosen for our design. We selected 850 MHz structure, based on a standing-wave superconducting cavities with the gradient of 10 MV/m. The accelerator consists of 20 SRF modules that accelerates the beam to one GeV in a single pass.

Driver linac cavities will use the energy recovery to reduce the RF power requirements to less than 5 kW per module. For our design we had decided to power four cryomodules by one 23 kW klystron YK1180 from Siemens. This is conventional CW klystron used in TV stations. Injector cavities and initial part of linac (first 50 MeV accelerator section) operating without energy recovery, will require about 600 kW RF power. For this active part of the SRF linac we selected 500 MHz structure based on standing-wave superconducting cavities with gradient of 5 MV/m. The value of 500 MHz was chosen since high power klystrons are commercially available for this frequency. An appropriate RF source is one 1000 kW TH2105 tube with electronic efficiency $\eta(\text{klystron}) \simeq 60\%$. This klystron is produced by Thompson for scientific applications.

The design of RF structure for RF lens is based on the need to minimize material costs and cryogenic losses. Electron bunches pass an RF lens

at 90°-crossing phase, so this RF structure is passive. The electron beam passes the RF lens only once. As a result, high-order mode losses are smaller in this case, and the problem of energy beam instabilities does not exist at all (contrary to the driving linac). Wakefield effects in the RF lens are not important due to large length of the bunch. Also, one should not care too much about the problem of emittance dilution in the energy-recovery loop.

Let us discuss the problem of choosing the RF frequency for the RF lens. Increase of the operating frequency of the RF structure leads to decrease of transverse dimensions of the devise and decrease of total voltage V_0 of the RF lens (see Section 2 more details). So, the cost of the RF lens scales with the RF frequency more strongly than that of the driving accelerator. Considering material costs for $f = 3$ GHz might appear to be the optimum, but there are compelling arguments for choosing a half of this frequency. First, non-linearity (aberrations) of the RF lens increases quadratically with the frequency.[2] Second, the maximum number of cells per cavity is limited by the requirements that higher-order modes must be extractable and no trapped modes be present. With requirements the number of HOM couplers increases with frequency. Following these arguments we select 1500 MHz structure based on standing-wave superconducting cavities with gradient of 10 MV/m. The RF lens consists of seven superconducting RF modules with total voltage $V_0 \simeq 350$ MV. RF lens cavities are passive. Thus, each cryomodule will use a 5 kW TH2466 klystron. This klystron is produced by Thompson for scientific applications.

3.3. Bunch compressors and electron beam transport

In order to achieve the high peak current in the undulator the bunch must be compressed in a series of magnetic chicanes. For the driver accelerator design we assume to use a three-stage compressor design. The first stage consists of a 500 MHz SRF section followed by a magnetic chicane generating the R_{56} needed for the bunch compression (the R_{56} is the (5,6) element in the linear transfer matrix). The magnetic chicane, located at a relatively low energy, compresses the bunch from $\sigma_z \simeq 4.2$ to 1.6 mm (see Fig. 8). The first stage of the SRF structure provides a total RF voltage of about 30 MV and operates with an off-crest phase.

Then, the beam is accelerated with an off-crest phase from the energy of roughly 30–150 MeV where it is injected into the second magnetic bunch compressor (see Fig. 9). The two magnetic chicanes compress the bunch from $\sigma_z \simeq 1.6$ to 0.45 mm.

After the second bunch compressor the bunch is accelerated with an off-crest phase to about 550 MeV where it is injected into the third magnetic bunch compressor. Like the second compressor, the third compressor is also a sequence of two magnetic chicanes. The third stage compresses the bunch to the final bunch length of $\sigma_z \simeq 0.15$ mm, before injection into the last part of linac, which accelerate the bunch with an on-crest phase up to 1 GeV.

Requirements for magnetic bunch compressors in our case are very close to those for magnetic bunch compressors in X-ray FELs [4]. In particular, the magnetic chicanes for the VUV FEL at TTF, which is presently under construction, is a good example for many problems related to our bunch compressor design [20]. Each 5 m long chicane contains four C-type bending magnets with a gap width of 3.5 cm and a good field region of about 20 cm. The bending magnets are rectangular magnets which do not have net focusing in the horizontal plane and therefore do not generate higher-order dispersion that would increase transverse emittance. Additionally, this design of bunch compressor is attractive because chicane introduces no net beamline bend angle and allows simple tuning with a single power supply. Each chicane can generate $R_{56} =$ 15–25 cm at deflection angle $\alpha = 15$–$25°$. The quadrupole triplets are placed between the chicanes in locations where the dispersion passes zero value. In this manner, they can constrain the beta functions but they will not generate any second-order dispersion and do not need large apertures. This eliminates the need for strong sextupole magnets. The magnetic bunch compressors are arranged and located such that non-linearities in the compression and acceleration

[2] The bunch length in the RF lens is limited by the condition for the energy spread be $\Delta E_f < 2$ MeV.

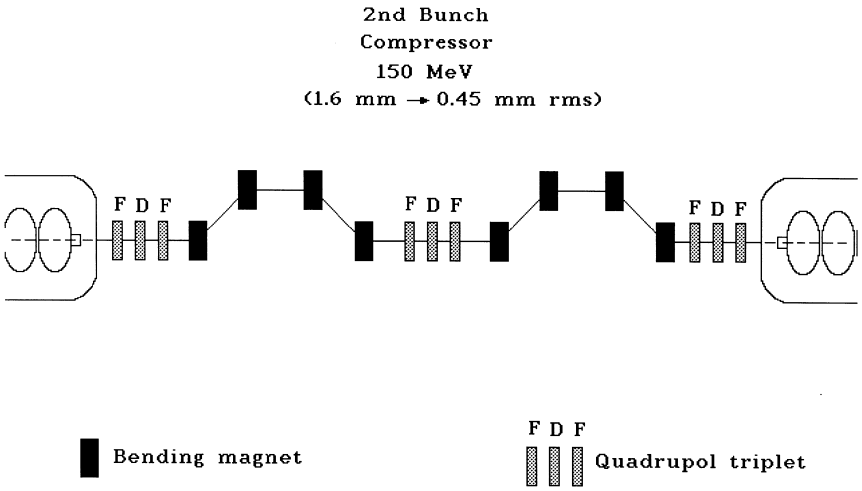

Fig. 9. Layout of the bunch compressor at stage 2.

process (RF curvature, space-charge effects, longitudinal wakefields and second-order momentum compaction) do not limit the achievable bunch parameters.

It should be noted that there are similarities between our design and TTF three-stage bunch compression system [14]. The first TTF magnetic bunch compressor is located directly after the 15 MeV, 1.3 GHz SRF accelerator (booster cavity) and compresses the bunch with $\sigma_z \simeq 1.6$ to 0.8 mm. The second TTF bunch compressor is located after the 150 MeV acceleration section and compresses the bunch with $\sigma_z \simeq 0.8$ to 0.28 mm. In the third stage the bunch is compressed to the final length of $\sigma_z \simeq 0.05$ mm at the energy of 500 MeV. The TTF bunch length scaled to the RF wavelength (i.e. $\sigma_z/\lambda_{\mathrm{rf}}$) and energy of the bunch are close to those required in our design. Compressing the bunch in the TTF will be done in stages to avoid space charge and coherent synchrotron radiation (CSR) effects limiting the achievable bunch length and transverse emittance. A calculation of the space-charge force in bunched beam shows that this should not be a serious limitation in the TTF case.[3]

[3] This is not completely true for the first bunch compressor. However, in the case under study the peak current of the bunch at the entrance of first compressor is smaller and the energy is higher comparing with the TTF case.

In contrast, the electric field of the CSR induces an energy variation along the bunch, i.e. the CSR field is similar to a longitudinal wake field. In the chicanes, this field will destroy the achromaticity of the compressor and the horizontal emittance will be increased. If we neglect the shielding effects of the vacuum chamber, the CSR-induced energy spread is predicted to be roughly [21]

$$\delta E/E \simeq 0.2 N r_{\mathrm{e}} L_{\mathrm{m}}/(\gamma R^{2/3}\sigma_z^{4/3})$$

where N is the number of the particles in the bunch, L_{m} and R are the bending magnet length and bending radius, and r_{e} and γ are the classical electron radius and the relativistic factor. The CSR is suppressed by vacuum chamber. The point where shielding becomes important can be estimated as $\sigma_z > h^{3/2}/R^{1/2}$, where h is the transverse size of the chamber. Comparing parameters of the TTF with our design we can conclude that to make preservation of the transverse emittance in the case of the TTF parameters is more difficult. On the one hand, normalized transverse emittance of the TTF beam ($\varepsilon_{\mathrm{n}} \simeq 2\pi$ mm mrad) is much smaller comparing with our design ($\varepsilon_{\mathrm{n}} \simeq 8\pi$ mm mrad). On the other hand, in our case the bunch length is of about 3 times larger. Thus, the chamber shielding in our case may more effectively reduce the predicted emittance dilution. This means that successful operation of the TTF will prove that high-quality

electron bunches with peak current of about few kA might be obtainable, and there is no need to built a special bunch compression facility for verifying the proof-of-principle.

The beam will be recirculated through two 180° arcs for further deceleration in the same SRF structures, to a minimum energy of about 10 MeV. In the undulator the energy spread in the beam is increased in the process of FEL interaction, to as much as $\Delta E_i \simeq \pm 50$ MeV. The first arc transport from the undulator to the driver linac is nonisochronous and optimized for an effective bunch decompression. After passing this arc the beam bunch is lengthened, and position of the particle along the bunch becomes correlated with the energy, i.e., we have the energy tilt along the bunch. That tilt is removed in RF lens, where energy spread is reduced to $\Delta E_f \simeq \pm 1.5$ MeV. The RF lens consists of a 1500 MHz SRF structure that provides a total RF voltage of 350 MV, and operates at the phase of $\phi_0 = 90°$. The first arc performs a decompression to the bunch length of $z_b \simeq 9$ mm. In the linearized limit, this implies: $R_{56}\Delta E_i/E \simeq 0.45$ cm, or $R_{56} \simeq 10$ cm. The quantity of R_{56} is naturally about few meters in a typical arc transport at this energy. In our case we desire it to be much smaller. To obtain the desired value of R_{56}, the lattice of the arc must be perturbed with the introducing, for example, of negative bends. In addition to R_{56} control, the arc transport must be achromatic. A compact, nearly isochronous lattice can be obtained using a "reverse-bend"-type lattice, originally developed in Ref. [22] and used at the DEMO facility [23]. This lattice consists of achromatic cells, each of which consists of a large positive bend, a set of matching quadrupoles, and a negative bend, followed by mirror image set of matching quadrupoles and positive bend (see Fig. 10). The combination of small dispersion (η) at the large bends and large tunable η at small negative-bends leads to nearly zero value of R_{56}.

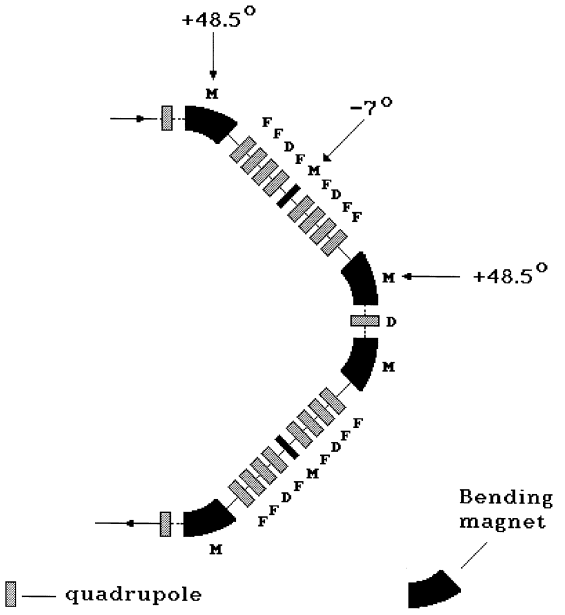

Fig. 10. Layout plot for return arc.

4. FEL amplifier

FEL amplifier is the key element of the proposed system which produces MW-level output radiation power. The operation of the FEL amplifier is based on the prolonged (resonance) interaction of the electron beam with the electromagnetic wave in the undulator. The amplification process can be divided into two stages, linear and non-linear. During linear stage of amplification, exponential growth of the electromagnetic field amplitude and of the beam modulation amplitude take place. Nevertheless, the beam modulation is much less than unity in the linear regime, and the largest fraction of the radiation power is produced at the non-linear stage of the operation, when the beam modulation becomes about unity. In the case of an uniform undulator the electron beam in the nonlinear regime is overmodulated, most electrons fall into accelerating phase, and the electron beam starts to absorb power from the electromagnetic wave. As a result, the efficiency of the FEL amplifier is limited by the value which is always much less than unity. A reliable method to prolong the interaction of the bunched electron beam with the electromagnetic wave and to increase the FEL efficiency consists in an adiabatic change of the undulator parameters (or in undulator tapering [24–27]). It has been shown that in the framework of the one-dimensional model optimal undulator

tapering occurs when the variation of the undulator parameters is a quadratic law [28,29]. The situation changes drastically if we take into account diffraction effects. In particular, the quadratic law of tapering no longer works in the three-dimensional case, and a linear law should be used [30].

The calculations based on the steady-state theory have shown that at the length of the undulator of 60 m, the efficiency of the UV FEL amplifier reaches the value of 10%. Nevertheless, at such a length of the undulator one should take into account the slippage effect. For instance, at the undulator period equal to 7 cm and the radiation wavelength equal to 260 nm, the kinematic slippage of the radiation with respect to the electron bunch is about 170 μm, which is comparable to the rms length of the electron bunch $\sigma_z = 150$ μm. So, the parameters of the FEL amplifier should be optimized using the time-dependent approach. Optimization of the parameters has been performed with the non-linear, three-dimensional, time-dependent simulation code FAST [11]. The optimized parameters of the UV FEL amplifier are presented in Table 1. The length of the untapered section of the undulator is equal to 18.4 m. At the operating wavelength of the FEL amplifier around 260 nm, the peak value of the magnetic field is about 1.15 T. The field in the tapered section is reduced linearly with the length from 1.15 T down to the value of 1.05 T at the end of the undulator of 60 m. Fig. 11 presents evolution along the undulator length of the energy in the radiation pulse. Fig. 12 shows the time structure of the radiation pulse at the exit of the undulator. We obtain that the duration of the radiation pulse is about 0.7 ps. The energy in the radiation pulse is equal to 83 mJ and the conversion efficiency (ratio of the energy in the radiation pulse to the energy in the electron pulse) is equal to 4.15% . The average power of the radiation from the FEL amplifier is equal to 500 kW. Analysis of the beam power losses along the electron bunch shows that the radiation is produced mainly by the front fraction of the electron bunch. This is natural consequence of the slippage effect mentioned above. On the other hand, one can see that the actual slippage of the radiation pulse is significantly less than the kinematic slippage, because the group velocity of the radiation in the electron beam is less

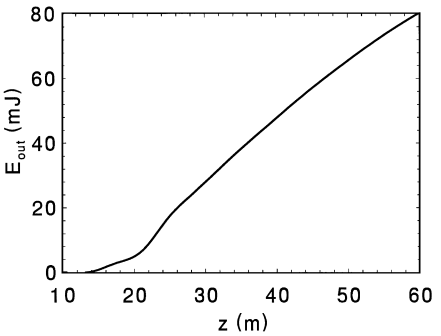

Fig. 11. Energy in the radiation pulse versus the length for the FEL amplifier.

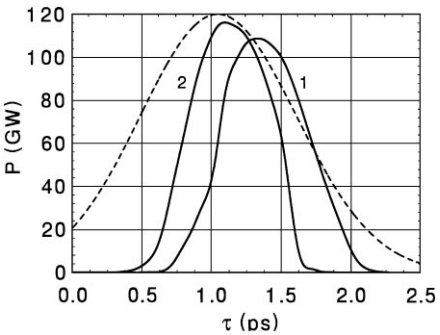

Fig. 12. Time structure of the radiation pulse at the exit of the FEL amplifier with tapered undulator (curve 1) and of the power loss in the electron bunch (curve 2). Dashed line is the longitudinal profile of the electron bunch (maximal value of the beam current is equal to 1.5 kA).

than the velocity of light (see Ref. [30] for more details). We see that this effect reveals an opportunity to achieve significant extraction efficiency even in the case when the electron bunch is short with respect to the kinematic slippage distance.

The phase analysis of the particles shows that the electrons of the central part of the bunch are well separated into two fractions, of about 70% of the electrons are trapped in the regime of coherent deceleration (see Fig. 13). However, the particles located at the tails of the bunch are not trapped in the regime of coherent deceleration, so the trapping efficiency averaged over bunch is about 40%. Fig. 14 presents the energy distribution in the electron beam at the exit of the undulator averaged over bunch. It is seen that the energy spectrum of

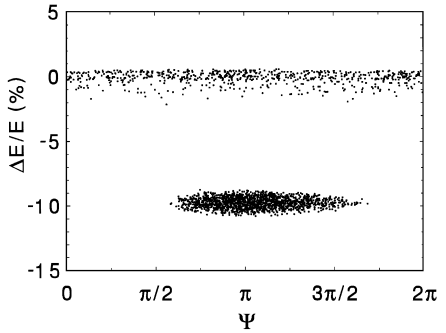

Fig. 13. Phase distribution of the particles in the middle of the electron bunch. Extraction efficiency of the FEL amplifier is equal to 4%.

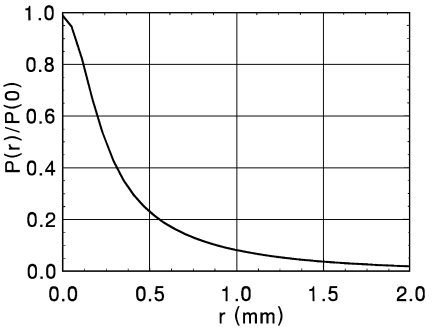

Fig. 15. Radial distribution of the radiation intensity at the undulator exit. Extraction efficiency of the FEL amplifier is equal to 4%.

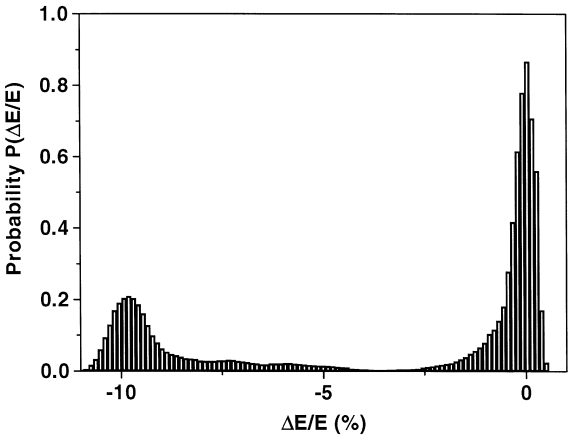

Fig. 14. Energy distribution of the electrons at the exit of the FEL amplifier. Extraction efficiency of the FEL amplifier is equal to 4%.

the spent beam is rather wide, about 10%. The radial distribution of the radiation intensity at the exit of the undulator is presented in Fig. 15. It is seen that there are long tails spanning up to the distance of about millimeter apart from the electron beam. This is caused by the diffraction effects.

5. Sensitivity and stability analysis

A sensitivity and stability analysis of the FEL amplifier operation has been performed using three-dimensional, time-dependent simulation code FAST. Each parameter of the electron beam at the undulator entrance was varied in turn, while all other parameters were held fixed, to establish how large a deviation could be tolerated in that single parameter. Limits on the tolerable deviations were determined by the tolerances on the output optical power. The optical power tolerance requirements were dictated in turn by the stability requirements on the electron beam energy at the undulator exit. The electron energy fluctuations are limited by the energy-recovery system, which requires that $\delta E < 1$ MeV. As a result, the constraint on the beam parameters at the undulator entrance is driven by the acceptable electron energy fluctuations at the undulator exit $\delta E/E < 10^{-3}$.

Sensitivity of the FEL amplifier operation to the deviation of the energy and charge (length) of the electron bunch, and deviations of the input laser power are illustrated in Figs. 16–18. First, we note that the FEL amplifier operation is insensitive to the deviations of the input laser power. It is seen that at the stability of the input laser power of about 10%, the stability of the energy in the output optical pulse is about 1% (i.e., stability of electron energy at the undulator exit is about 0.05%). The FEL amplifier operation is insensitive also to the time jitter of the input laser pulses. The top of the master laser pulse of duration 10 ps can be easily tuned to the arrival time of the short electron bunch having predicted absolute jitter of less than 3 ps. The absolute time jitter of master laser pulses of about 1 ps can be routinely provided with available laser technique.

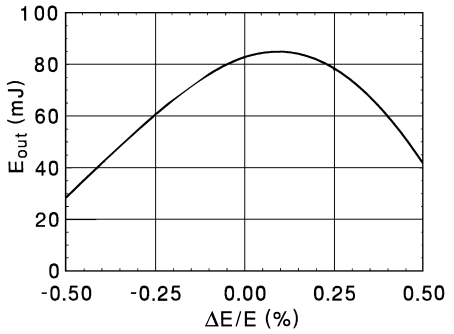

Fig. 16. Dependence on the energy deviation from exact FEL resonance of the energy in the radiation pulse of the FEL amplifier with tapered undulator. Extraction efficiency of the FEL amplifier at $\Delta E/E = 0$ is equal to 4%.

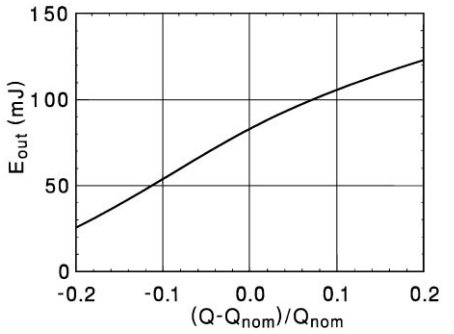

Fig. 17. Dependence of the energy in the radiation pulse on the bunch charge for the FEL amplifier with tapered undulator. Extraction efficiency of the FEL amplifier at $Q = Q_{\mathrm{nom}}$ is equal to 4%.

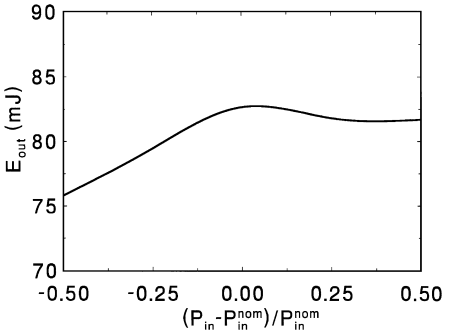

Fig. 18. Dependence of the energy in the radiation pulse on the input radiation power for the FEL amplifier with tapered undulator. Extraction efficiency of the FEL amplifier at $P = P_{\mathrm{in}}^{\mathrm{nom}}$ is equal to 4%.

In Fig. 16 we present the dependence of the energy in the optical pulse as a function of the deviation of the electron energy from exact FEL resonance. It is seen that at the designed stability of the energy of the driver accelerator ($<$ 0.1%), the fluctuations of the energy in the optical pulses are about 1% (i.e., relative energy deviation of electrons at the undulator exit is less than 0.05%).

Sensitivity of the output optical power to the deviations of the bunch charge is illustrated with Fig. 17. By means of recalculating the bunch charge deviation into the bunch length deviation simply as $\delta q/q = \delta\sigma_z/\sigma_z$, we can estimate the tolerance on the bunch length fluctuations.[4] The maximum tolerable bunch charge and bunch length fluctuations are both $(\delta q/q,\ \delta\sigma_z/\sigma_z) < 2\%$. Results of a stability analysis of the injector are presented in Ref. [6]. Table 3 summarizes the injector tolerance requirements in our case. The charge stability ($<$ 2%), bunch length stability ($<$ 2%), and bunch timing stability ($<$ 3 ps) impose the tightest limits on the injector parameters. The resulting requirements are shown in the last column in Table 3. It should be noted that the RF stability of injector bunchers we required has been demonstrated both in the amplitude and phase [6]. RF control of superconducting linac used by CEBAF has demonstrated stability at the level we require, namely, 5×10^{-5} in the amplitude and 0.1° in phase. For our design, we have adopted the CEBAF RF feedback system. Energy-recovery linac can, in principle, exhibit instabilities in the beam energy. These instabilities arise from fluctuations of the cavity fields. Coupling from the beam energy to the current and phase is included via beam loss on aperture (scraping) and non-zero compaction factor. Both effects change the beam-induced voltage in the cavities. Depending on the RF feedback characteristics this can lead to the instabilities of the accelerating field. Stability analysis of the SRF energy-recovery linac with CEBAF feedback system has been performed in Ref. [31]. It

[4] In our case the electron beam has a pulse duration comparable with the kinematic slippage of the radiation with respect to the electron bunch, and the question arises when one can use this simple relation. Results of numerical simulation show that the slippage effect is less important than the effect of fluctuation of the peak current.

Table 3
Results of a stability analysis of the injector

	Tolerance on injector output			
	Charge $< 2\%$	Bunch length $< 2\%$	Bunch timing < 3 ps	Derived requirement
Gun pulser phase (deg)	5.2	2.0	32	2.0
Buncher 1 phase (deg)	0.44	0.12	0.14	0.12
Buncher 2 phase (deg)	0.50	0.68	1.3	0.50
Four-cell phase (deg)	0.64	0.56	1.4	0.56
Gun voltage (kV)	0.50	0.56	0.75	0.50
Buncher 1 amplitude (kV)	3.8	2.32	4.7	2.32
Buncher 2 amplitude (kV)	2.2	2.0	2.3	2.0
Four-cell amplitude (MV/m)	0.4	0.27	0.15	0.15
Gun current (%)	2	2.32	21	2.0
Gun bunch length (%)	0.52	1.76	8.2	0.52

was found that, for small variations, modest gain frequencies, well within CEBAF's RF control system capability, are required to stabilize the system. Recently, according to the schedule of Phase I, Jefferson Lab's energy-recovery SRF linac has exceeded design specifications. It achieved 48 MeV of beam energy with 4 mA of average beam current. No signature of longitudinal instabilities was observed, in agreement with the modeling predictions [32,33]

6. The undulator

The undulator is one of the central components of the UV FEL amplifier. It has two functions. First, it has to provide the sinusoidal field, so that the FEL process can take place. The values for the peak field and the period length are given in Table 1. Second, additional focussing is required in order to keep the beam size small over the whole undulator length. A quadrupole lattice consisting of focussing and defocussing quadrupolar fields (FODO lattice) has to be provided. Requirements for this device in our case are very close to the undulators in X-ray FELs [4,5]. In particular, the 30 m long undulator for the X-ray FEL at the TTF, which is presently under construction, is a good working example for many problems related to our undulator design [14,17,34,35].

The required field strength can be achieved using Halbach's hybrid configuration [36]. The term "hybrid" means that soft iron pole pieces are used in conjunction with Nd–Fe–B permanent magnets. This principle is widely used in the undulator technology. At a gap of 12 mm, peak field up to 1.5 T is feasible for the undulator period $\lambda_u = 70$ mm. This is more than needed for the UV FEL amplifier undulator.

Tolerances for the field errors and alignment are estimated on the basis of work done for the undulator for X-ray FEL at TTF. First, there should be distinguished steering errors, which deflect the electron beam out of the overlap region between the electron beam and laser field. This overlap plays a key role for the FEL performance and can be described by the second field integral. The source of steering errors is caused by magnetic errors of the poles, magnetization, homogeneity and angle errors of permanent magnets. The field integral of one period is not zero anymore and the mean trajectory may deviate from a straight line. There is a close relation between the horizontal and vertical orbit excursions and the second field integral, which can be derived from the magnetic measurements. Again, the overlap must not be disturbed by more than 20% of the beam size.[5] In the case under

[5] In the case of an X-ray FEL the transverse dimensions of the electron and photon beam are almost identical and are about 25–50 μm. This requires to maintain the electron trajectory with an accuracy of about 5–10 μm. Even this problem can be solved [4].

study the size of the electron and photon beam is about 100 and 300 μm, respectively. This means that the mean electron trajectory should not deviate from a straight line by more than 50 μm, corresponding to a second field integral error of $I_2 < 170$ T mm^2. These requirements placed on the undulator are not very stringent. Experience with undulators for synchrotron radiation sources (SRS) and FELs shows that this should not be difficult to obtain. For the 15 m VUV FEL undulator at the TTF the second field integral $I_2 = 10$ T mm^2 has been obtained [35].

There may also be distortions in the periodicity of the field that do not deflect the beam at all but rather change the phase of the electron with respect to that of laser field. The phase jitter induced in this way, is called as RMS phase shake, $\Delta\phi_{\mathrm{RMS}}$ [37]. The optical phase shake can be derived from the magnetic measurements. The acceptable phase shake for the UV FEL undulator can be estimated as $\Delta\phi_{\mathrm{RMS}} < 0.2 \simeq 12^\circ$. This also should not be difficult to obtain. For the undulator at SRS the value of $\Delta\phi_{\mathrm{RMS}} \simeq 6^\circ$ has been obtained [4].

Simulations of the FEL amplifier shows that strong focusing must be added to the undulator lattice in order to maintain a small beam size. Natural focusing would give a beta-function length of about 7.5 m, while optimal focusing occurs with a beta-function of less than 3 m. It is possible to combine the generation of the periodic undulator field which is needed for the FEL process with the generation of the quadrupolar field which is needed for strong focusing. Permanent magnet technology offers solution for this problem. The undulator for X-ray FEL at the TTF uses this principle [17]. In our case at a gap of 12 mm the alternating gradient field is about $\pm$ 20 T/m, quadrupole length is 14 cm and FODO cell length is 1 m. It should be noted that X-ray FEL undulator at the TTF has completely the same parameters of strong focusing system [35].

In a combined function undulator the tight alignment tolerances of a 50 μm for quadrupole alignment has to be met by the devise as a whole. Within each module the individual quadrupoles have to be measured and trimmed to be on a common axis. Different modules have to be aligned with this precision with respect to each other. These geometrical alignment tolerances in the order of 50 μm for the quadrupole elements seem to be not challenging. For the 15 m VUV FEL undulator at the TTF the horizontal and vertical quadrupole positions are aligned better than 50 μm rms [38]. The tight alignment tolerances can be achieved using the beam-based alignment technique, which has been successfully demonstrated at the Final Focus Test Beam (FFTB) at the Stanford Linear Collider (SLC) [39]. Correction techniques, such as beam-based alignment, and appropriate corrector coils will be used at X-ray FEL at the TTF to achieve 10 μm accuracy [40].

Proposed undulator has a planar geometry which is a big advantage for the manufacturing, magnetic measurement, installation of vacuum chamber, beam diagnostics, etc. Variation of the gap to tune the photon energy is not required. This can be done by changing the energy of the electron beam. A fixed taper of the undulator is required allowing for a reduction of the undulator K parameter of 10% over the whole undulator length, compensating for the losses of average kinetic energy transferred to the laser light. This prolongs the interaction of the bunched electron beam with the laser wave and increases output optical power. The whole undulator system will be subdivided into 12 modules. Each module requires 5.2 m; 4.9 m for the magnet structure (70 undulator periods and 5 FODO periods), and 0.3 m for the matching section. The separation between two sections of the FEL undulator is given by the condition that, as the electron and optical wave travel the distance d_{sep}, the phase of the wave advances by $\Delta\phi = 2\pi$. As a result, d_{sep} is given by: $d_{\mathrm{sep}} = \lambda_{\mathrm{u}}(1 + K^2/2)$, and d_{sep} is independent of the radiation wavelength and electron energy. In our case minimal length of the drift space d_{sep} is equal to 2 m. Such long interruptions will have a strong effect on the FEL process due to the loss of the power in the laser field caused by diffraction. Therefore, a special magnet phase shifter between the modules is needed which decreases d_{sep} from 2 to 0.3 m [41]. The separation will be used for diagnostics, steering corrector magnets, pumping ports and other equipment which does not fit inside the undulator gap.

The beam position monitor (BPM) system is the primary system for measuring the transverse position of the electron beam in the undulator. The BPM system is used to maintain co-linearity of the electron and photon beams, within 50 μm rms over the whole undulator length. The absolute accuracy of the BPM system is the basis of the alignment system. The initial survey errors of BPM detector are held to better than 50 μm. Each BPM must have the ability to detect relative changes in position of 10 μm at the nominal operating charge of 1 nC bunches. These requirements placed on the BPM system are not very stringent and are within the forefront of position measurement technology. For example, the microwave cavity BPM detector, installed in the TTF X-ray undulator, can provide resolution at a micron level absolute accuracy [42]. It should be noted that it is the non-interception monitor.

7. Output optical system

Peak and average optical power at the exit of FEL amplifier are about 100 GW and 0.5 MW, respectively. To provide the possibility of application of conventional optical elements, the laser beam is expanded from the size of about 1 mm (at the undulator exit) up to the size of 30 cm. Such an expansion is performed in two steps. At the first step the beam should be expanded diffractionally up to the size of 3 mm. The required size of the laser beam is obtained at the distance of the drift space equal to 30 m. After the step of diffraction expansion, the laser beam is directed to the hyperbolic mirror and is expanded further up to the size of 30 cm. We choose the incident angle on the mirror corresponding to $\cos\theta \lesssim 10^{-2}$. To reduce the heat losses in the mirrors, we use the fact that the radiation absorption at the grazing reflection depends strongly on the polarization of the radiation. In the case of a large value of the refractive index n (i.e., $|n|^2 \gg 1$), the relative absorption for TE wave (electrical field is perpendicular to the reflection plane) is given by the expression [43]

$$A_s \simeq 4n_1 \cos\theta/(n_1^2 + n_2^2),$$

where θ is the incident angle ($\cos\theta \ll 1$ at the grazing incident), $n_1 = \mathrm{Re}\, n$, and $n_2 = \mathrm{Im}\, n$. The relative absorption for TM wave is larger than A_s approximately by a factor of $|n|^2$:

$$A_p \simeq 4n_1 \cos\theta.$$

Remembering the fact that the FEL radiation in our case (planar undulator) is completely linear polarized we have a possibility to use this opportunity to decrease heat losses in the mirror. Let us present specific example for visible range of spectrum. For Ag mirror and green light the absorption coefficient for TM wave is by 10 times larger than that for TE wave, since $n_1 \simeq 0.05$ and $n_2 \simeq 3.3$ in this case. In our case, the heat losses in the Ag mirror at $\cos\theta \simeq 10^{-2}$ and wavelength $\lambda \simeq 500$ nm are about 10 W/cm^2 only. The angle divergence of the optical beam after the mirror is about $\Delta\theta \simeq \cos\theta \simeq 10^{-2}$, so at the distance of 30 m the size of the laser beam will achieve the required value of 30 cm.

An important problem is that of extracting the powerful laser beam into the atmosphere. We propose to perform such an extraction at the stage of diffraction expansion of optical beam (the length of the channel is 30 m). The idea is to organize a transformation from pressure of 10^{-8} Torr inside the vacuum chamber of the FEL amplifier up to the atmospheric pressure in the vicinity of expanding hyperbolic mirror. To solve this problem, we use the extractor with differential evacuation [44]. Such an extractor (see Fig. 19) may consist of several chambers separated by diaphragms. At the initial stage of the laser beam expansion the aperture of diaphragms is of about 5 mm. One should also keep in mind a possible problem of the laser discharge in the output channel, since we deal with a high-intensity laser beam. First, we remember that the threshold of the laser discharge decreases with the gas pressure. For instance, for N_2 gas, this threshold is $P_{th} \simeq 10^{14}$ W/cm^2 at a pressure of 1 Torr, and is $P_{th} \simeq 10^{13}$ W/cm^2 at the pressure of 10^3 Torr. In our case at the entrance of extraction channel the peak flux is about 10^{13} W/cm^2, and at the exit of the channel is about 10^{12} W/cm^2, i.e. by an order of magnitude less than the discharge threshold for N_2 along the whole length of the channel.

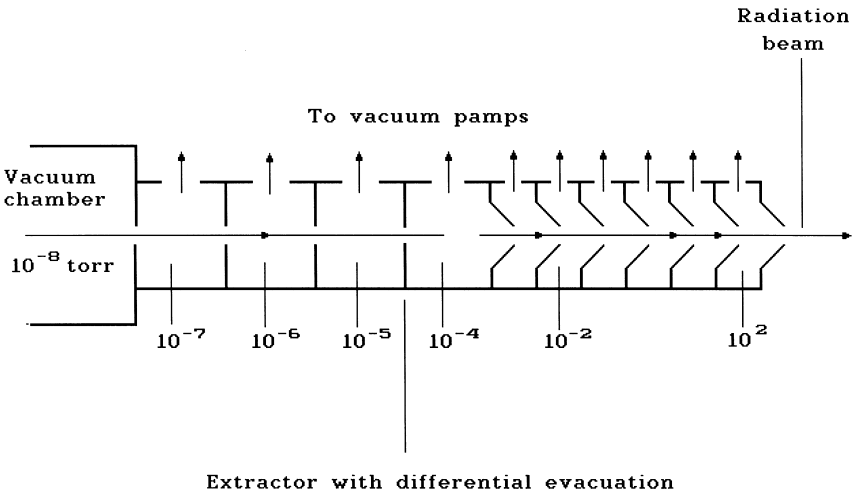

Fig. 19. Extractor of radiation beam.

8. Future potential

8.1. Upgrade to higher power

Analysis of parameters of a high-power UV FEL shows that its average output power is clearly limited by the value of average current achievable with injector and SRF accelerator cavities. In order to go to power beyond $P_{av} \simeq 0.5$ MW, the bunch repetition rate would therefore be increased. To obtain a high value of average beam current without injector hardware modifications, we use the beam summation system [45,46] which combines the beams with average current $I_0 = 12.2$ mA produced by four preaccelerators into one beam with average current of $I = 4I_0 \simeq 50$ mA. This is performed in two stages (see Figs. 20 and 21). At each stage two electron beams with different energies of electrons are combined and then their energies are equalized in a special RF accelerator structure (equalizer). Each preaccelerator consists of an injector (identical to that described in Section 3.1), and SRF accelerator module. Injectors operate with the repetition rate of $f_0 \simeq 6.1$ MHz, and RF frequency of the cavities is equal to $f_{rf} = 80f_0 \simeq 500$ MHz.

The first stage of the beam summation system operates as follows. Electron beams from two preaccelerators with different energies E_1 and $E_2 = E_1 + \Delta E$ are combined into one train by means of bending magnets system (combiner). At the exit of the combiner the bunch repetition rate is equal to $f_{rep} = 2f_0$. Then the electron beam is directed to the RF accelerator structure operating at $f_{rf} = 79f_0$. The phasing is chosen in such a way that the bunches with a higher and lower energies are located in the minimum and maximum of the RF acceleration field, respectively. As a result, at the exit of the equalizer we have monoenergetic electron beam.

The second stage operates in the same way. First, the beams with different energies are overlapped with each other. At the exit of the combiner the bunch repetition rate is equal to $f_{rep} = 4f_0$. To equalize the energies, the RF frequency of the second equalizer is chosen to be $f_{rf} = 78f_0$. The total voltage of three RF accelerator–equalizer is relatively small. The RF power in these accelerator structure is not used. As a result, the energy consumption and cost of the accelerators–equalizers is much less than that of preaccelerators. Each preaccelerator operating without energy recovery requires about 600 kW of RF power provided by one TH2105 tube.

The key advantage of this scheme is that each preaccelerator is basically initial part of driver linac described in Section 3. As a result, no modifications

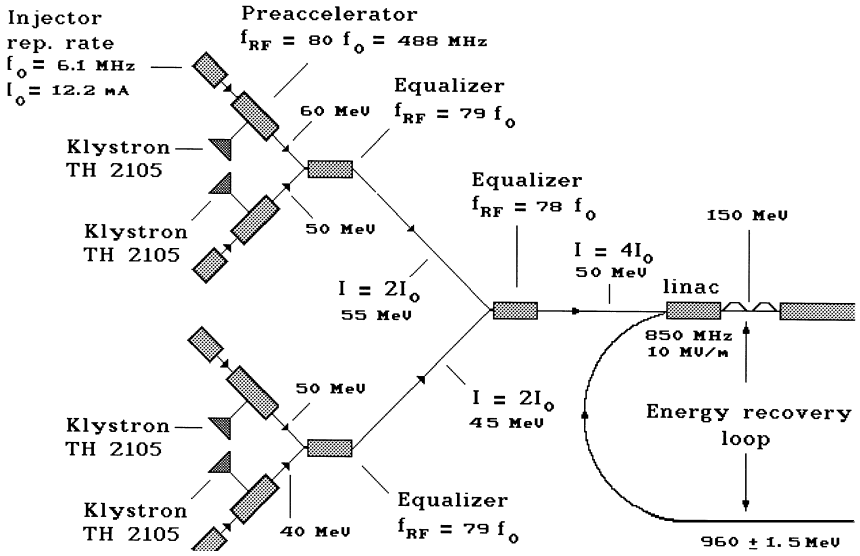

Fig. 20. The scheme of the electron beam summation system.

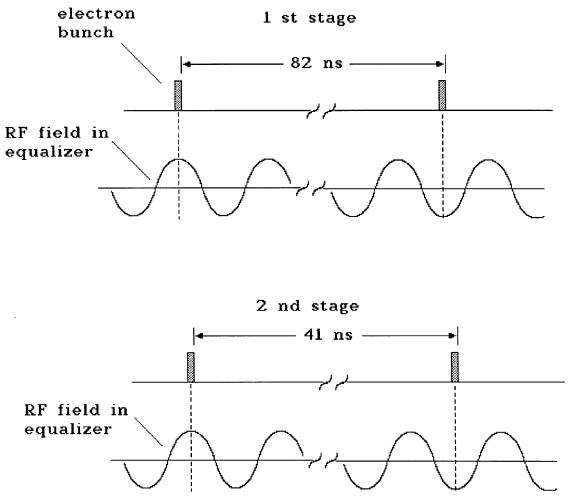

Fig. 21. The scheme of operation of the energy equalizers.

are necessary for the injector and for the SRF cavities which operate without energy recovery. In this high average current scheme only driver linac cavities use the advantage of the energy-recovery. The modifications of these cavities are driven only by the increase in high-order mode power resulting from the increase of average current.

8.2. Photon energy upgrade

An attractive feature of the FEL amplifier scheme is the absence of no apparent limitation which would prevent operation at even VUV wavelength range. Since the amplification process develops in vacuum during one pass of the electron beam through the undulator, the problem of the absorption of the radiation in the mirror and active medium in the FEL amplifier does not exist at all. On the other hand, the physical principles of the FEL amplifier operating in the VUV wavelength band are the same as those in the UV range. The requirements are that the parameters of the electron beam and undulator become more severe when going down to shorter wavelength. However, these requirements evolve slowly with the operating wavelength. It has been mentioned previously that decreasing the radiation wavelength also decreases the maximum tolerable transverse and longitudinal beam emittances. Thus, improving the driver linac injector towards even smaller beam emittances will be an issue for any photon energy upgrade. For the UV FEL amplifier, described above, we have adopted very conservative design for the injector. That design is based on a convectional thermionic cathode, subharmonic bunchers,

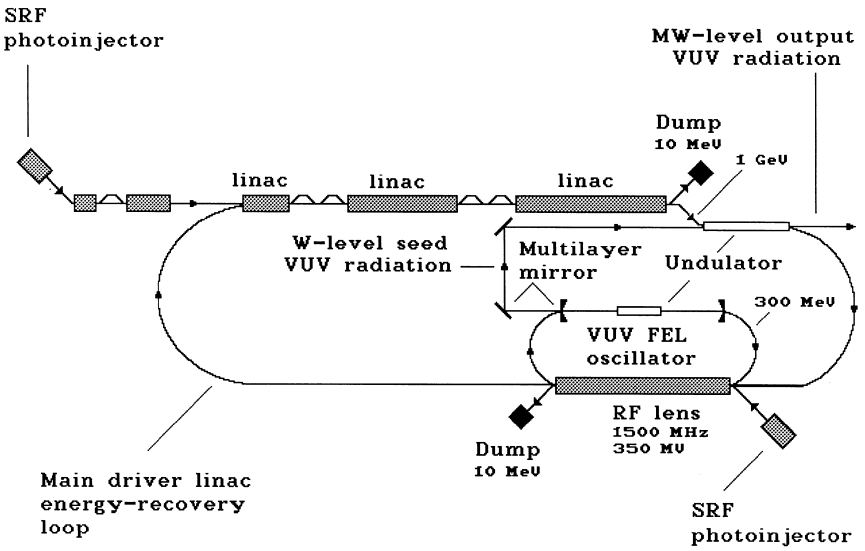

Fig. 22. Schematic illustration of design configuration for the VUV FEL amplifier.

and fundamental acceleration. Nevertheless it is possible to meet or exceed all of the industrial-use UV FEL design requirements with this approach.

For MW-scale VUV FEL amplifier a new approach that was considered would have made use of an RF superconducting cavity with an internal photocathode. This approach entails using a cryogenic photocathode in a high-gradient half-cell superconducting structure. The laser pulse length would be about 10 ps, and the accelerating gradient would be 25–30 MV/m at the photocathode. This approach would have to eliminate most of the difficulties associated with the space-charge forces in the adopted design. The SRF photoinjector will produce electron beam emittance sufficiently low to meet the constraints implied by VUV FEL amplifier requirements (Normalized transverse emittance $\varepsilon_n \simeq 4\pi$ mm mrad., longitudinal emittance $\varepsilon_l \simeq 50$ keV mm at charge per bunch 1–2 nC). SRF photoinjector configuration is being developed for example at FZR (Rossendorf) [47,48]. This technology may be mature within five years, though many uncertainties remain. CW operation photocathode requires, in our case, the laser with a relatively high average power (about 100 W at 527 nm). However, the field of CW mode-locked Nd glass laser design is moving forward rapidly, a 10 W level lasers are now commercially available, and a 100 W level of average output power does not seem to be a challenging problem.

The master laser oscillator system is of critical importance to the overall performance of the VUV FEL amplifier. Nowadays we have the situation that the wavelength range below 200 nm is not covered by quantum lasers. The main problem is that radiation absorption in the active medium increases drastically when approaching the VUV band. The plausible approach would have made use of VUV FEL oscillator as a master laser. This device, pictured in Fig. 22, incorporates a recirculating SRF 1500 MHz accelerator comprising a 10 MeV injector (SRF gun with photocathode) and 350 MeV energy-recovery linac to produce electron beam for CW watt-level lasing. It is assumed that the master FEL oscillator and energy-recovery driver linac design will be the same as those now being used in UV FEL at Jefferson Laboratory [1]. Our FEL-accelerator configuration would use the RF lens structure in energy-recovery loop of the main driver accelerator as a linac (see Fig. 11). As a result, the VUV FEL master oscillator would be reasonably cost-effective.

The performance of the optical cavity components are of key importance for the success of the VUV FEL oscillator. Although it will have only watt-level of the average output optical power, one should care about the problem of the radiation load on the mirrors. Namely, the peak power will be very high and the effect of shock radiative treatment on the optical elements is not easily estimated. This is a new challenge for mirrors and multilayers. Systematic studies of the effect of the high peak power of the laser pulses during very short time intervals on the optical components are needed. The Material Department of the GKSS Forchungszentrum now concentrates on the development and test of the mirrors and multilayers for the VUV and soft X-ray wavelength range [49,50]. This activity is considered as a start of a long-term program in context with the construction and operation of VUV and soft X-ray FEL seeding options at the TESLA Test Facility at DESY [51,52]. This activity will be of a great importance for the master VUV FEL oscillator instrumentation.

Acknowledgements

We thank J.R. Schneider, D. Trines and A. Wagner for their interest in this work, and B. Dwersteg, J. Pflüger, and J. Sekutowicz for many useful discussions and recommendations on technical topics. We are grateful to S. Wipf for careful reading of the manuscript.

References

[1] G.R. Neil et al., Nucl. Instr. and Meth. A 358 (1995) 159.
[2] S.V. Benson et al., Nucl. Instr. and Meth. A 429 (1999) 27.
[3] S.V. Benson et al., Nucl. Instr. and Meth. A 375 (1996) ABS 4.
[4] R. Brinkmann et al. (Eds.), Conceptual Design of 500 GeV e^+e^- Linear Collider with Integrated X-ray Facility, DESY 1997-048, ECFA 1997-182, Hamburg, May 1997.
[5] The Linac Coherent Light Source (LCLS) Design Study Report, SLAC-R-521, 1998.
[6] K.-J. Kim et al., LBL preprint Pub-5335, 1992.
[7] C. Yamanaka, Nucl. Instr. and Meth. A 318 (1992) 1.
[8] P.P. Pronko et al., Phys. Rev. Lett. 83 (1999) 2596.
[9] E.E. Haller, J. Appl. Phys. 77 (1995) 2857.
[10] A.J. Lichtenberg, Phase-Space Dynamics of Particles, Wiley, New York, 1969.
[11] E.L. Saldin, E.A. Schneidmiller, M.V. Yurkov, Nucl. Instr. and Meth. A 429 (1999) 233.
[12] R.A. Jong, W.M. Fawley, E.T. Scharlemann, SPIE 1045 (1989) 18.
[13] S. Reiche, Nucl. Instr. and Meth. A 429 (1999) 243.
[14] A VUV Free Electron Laser at the TESLA Test Facility: Conceptual Design Report, DESY Print TESLA-FEL 95-03, Hamburg, DESY, 1995.
[15] M. Hogan et al., Phys. Rev. Lett. 81 (1998) 4867.
[16] E.L. Saldin, E.A. Schneidmiller, M.V. Yurkov, Nucl. Instr. and Meth. A 429 (1999) 197.
[17] J. Pflueger, Y.M. Nikitina, Nucl. Instr. and Meth. A 381 (1996) 554.
[18] C. Pagani et al., Nucl. Instr. and Meth. A 423 (1999) 190.
[19] TESLA Test Facility – Conceptual Design Report, TESLA Report 95-1, DESY 1995.
[20] T. Limberg et al., Nucl. Instr. and Meth. A 375 (1996) 322.
[21] Ya.S. Derbenev et al., DESY Print TESLA-FEL 95-05, Hamburg, 1995.
[22] A. Amiry, C. Pellegrini, Proceedings of the Workshop on Fourth Generation Light Sources, SSRL92/02, 1992.
[23] D. Neuffer et al., Nucl. Instr. and Meth. A 375 (1996) 123.
[24] N. Kroll, P. Morton, M. Rosenbluth, SRI Rep. JSR-79-01, IEEE J. Quantum Electron. QE-17 (1981) 1436.
[25] C.M. Tang, P. Sprangle, Phys. Quantum Electron. 9 (1982) 627.
[26] D. Prosnitz, A. Szoke, V.K. Neile, Phys. Rev. A 24 (1981) 1436.
[27] T.J. Orzechowski et al., Phys. Rev. Lett. 57 (1986) 2172.
[28] R. Bonifacio et al., La Riv. Nuovo Cimento 13 (9) (1990) 1.
[29] E.L. Saldin, E.A. Schneidmiller, M.V. Yurkov, Sov. J. Part. Nucl. 23 (1992) 104.
[30] E.L. Saldin, E.A. Schneidmiller, M.V. Yurkov, The Physics of Free Electron Laser, Springer, Berlin, 1999.
[31] L. Merminga et al., Nucl. Instr. and Meth. A 429 (1999) 58.
[32] G.R. Neil et al., Nucl. Instr. and Meth. A 445 (2000) 192.
[33] L. Merminga et al., Proceedings of the 21st International FEL Conference, Hamburg, Germany, 1999, Elsevier, Science B.V., Amsterdam, 2000, p. II-3.
[34] B. Faatz, J. Pflueger, Y.M. Nikitina, Nucl. Instr. and Meth. A 393 (1997) 380.
[35] J. Pflueger, H. Lu, T. Teichmann, Nucl. Instr. and Meth. A 429 (1999) 386.
[36] K. Halbach, J. Phys. C1 (Suppl. 2) (1983) C11.
[37] R.P. Walker, Nucl. Instr. and Meth. A 335 (1993) 328.
[38] J. Pflueger et al., Magnetic characterization of the undulator for the VUV-FEL at the TESLA test facility, Proceedings of the 21st International FEL Conference, Hamburg, Germany, 1999, Elsevier Science B.V., Amsterdam, 2000, p. II-87.
[39] T. Tennenbaum et al., SLAC-PUB 95-6769 (1995).
[40] K. Floettmann et al., Nucl. Instr. and Meth. A 416 (1998) 152.
[41] J. Pflueger, private communications.

[42] R. Lorenz, T. Kamps, M. Wendt, Proceedings of the DIPAC 97, Frascati, Italy, p. 73.
[43] S. Solimeno, B. Crosignani, P. DiPorto, Guiding, Diffraction and Confinement of Optical Radiation, Academic Press, New York, 1986.
[44] E.A. Abramian, Industrial Electron Accelerators and Applications, Hemisphere, Washington, 1988.
[45] E.L. Saldin et al., preprint JINR E9-96-68.
[46] E.L. Saldin et al., Fusion Eng. Des. 44 (1999) 341.
[47] D. Jansen et al., Conference Proceedings of Particle Accelerator Conference, Vancouver, Canada, 1997.
[48] F. Gabriel et al., Nucl. Instr. and Meth. A 429 (1999) II 91.
[49] C. Michaelsen, K. Barmak, T. Weihs, Appl. Phys. 30 (1997) 3167.
[50] G. Wiener et al., Rev. Sci. Instr. 66 (1995) 20.
[51] J. Feldhaus et al., Opt. Commun. 140 (1997) 341.
[52] B. Faatz et al., Nucl. Instr. and Meth. A 429 (1999) 424.